Spin-polarized electronic and transport properties of $[V(Bz)_2]_n$@SWBNNT and $[V(Bz)_2]_n$@DWBNNT nanocables

YONGFANG SUN, CUICUI SUN, GUILING ZHANG*, YAN SHANG
College of Chemical and Environmental Engineering, Harbin University of Science and Technology, Harbin 150040, China

We have investigated electronic and transport properties of a novel form of $[V(Bz)_2]_n$@SWBNNT and $[V(Bz)_2]_n$@DWBNNT nanocables by means of density functional theory (DFT) and nonequilibrium Green's function (NEGF) methods. It is found that endohedral encapsulation of $[V(Bz)_2]_n$ into SWBNNT or DWBNNT could introduce magnetism for the hybrid nanocables. More importantly, the ferromagnetic state of the two nanocables is predicted to have a very high Curie or Neél temperature of over 1000 K, suggesting a potential candidate as magnetic nanopart. Transport properties of $[V(Bz)_2]_n$@SWBNNT and $[V(Bz)_2]_n$@DWBNNT are mainly controlled by the core $[V(Bz)_2]_n$ nanowire and present a half-metallic character. Values of the spin-filter efficiency of $[V(Bz)_2]_n$@SWBNNT and $[V(Bz)_2]_n$@DWBNNT amount to more than 60%, which may be viewed as a new kind of spin filter. Encapsulating $[V(Bz)_2]_n$ into either SWBNNT or DWBNNT can effectively tune electronic and transport properties and these nanocables can be potentially used as functional nanodevices.

(Received August 25, 2016; accepted April 6, 2017)

Keywords: Spin polarized, $[V(Bz)_2]_n$@SWBNNT, $[V(Bz)_2]_n$@DWBNNT, Transport property

1. Introduction

Boron nitride nanotubes (BNNTs) are suggested as ideal endohedral filling materials to fabricate 1D hybrid nanomaterials, X@BNNT, where X denotes the fillers. Functionality of these hybrid nanostructures can be broadened compared to that of single-component BNNT or encapsulated specie due to the interplay between them. BNNTs are insulators independent of their chirality and diameter and possess the potential for nanoscale electronic devices owing to their special properties that are useful in many fields [1]. With their band gap as high as 5.5 eV, it is expected to protect the encapsulated content from outside interference effectively [2]. In fact, many materials such as metal and alloy nanowires (Cu, Fe, Ni) [3-8], Mo clusters [9], halide potassium [10], silicon-containing nanowires (Si, SiC, Si/SiO_2, or SiC/SiO_2) [11-15], GaN nanowires [16-19], ZnS nanowires [20], and $Al_{18}B_4O_{33}$ nanowires [21] have been introduced inside single-walled BNNTs (SWBNNTs). Also, it has been found that BNNT coating is an effective way to improve the optical and field emission properties of Si tips [14], SiC nanowires [15], and GaN nanowires [17-19]. Further investigations using first-principles calculations demonstrate that multi-walled BNNTs (MWBNNTs) present better stability than SWBNNTs [22]. Indeed, this result was experimentally confirmed by Fuentes et al. [23] and Golberg et al. [24,25] However, study on filling of MWBNNTs is rather scared. From a fundamental viewpoint, DWBNNTs represent the simplest form of a MWBNNT, which makes them ideal candidates for investigating the effects of the interwall coupling between component nanotubes. Therefore, investigating filling effect upon DWBNNTs may offer some clues on understanding that for MWBNNTs.

Metallocenes are well known for their intriguing physical phenomena arising from transition metals. Particularly, ferromagnetism observed in V and Bz based mutidecker sandwich-like clusters (V_nBz_{n+1}) [26,27] and infinite wire $[V(Bz)]_n$ [27] results in their great promise as candidates for spin-polarized transport and information storage [28-30]. For such 1D systems, studies have been extended to another kind of metal-ligand complexes where the ligands being of polycyclic aromatic hydrocarbons [31,32]. Theoretical studies predict that these sandwich-like wires exhibits better stability and conductivity than that of $[V(Bz)]_n$, and thus may be more suitable for real applications [33]. Polyphenylene provides a perfect polycyclic aromatic chain for sandwiching V atoms to form 1D vanadocene nanowires $[V(Bz)_2]_n$. Furthermore, BNNT provides an ideal interior space for

fabricating $[V(Bz)_2]_n$.

In this work, we investigate electronic and transport properties of a novel kind of nanocables by inserting $[V(Bz)_2]_n$ into SWBNNT and DWBNNT. To our knowledge, this is the first contribution for these nanocables. Our results show that the two nanocables are thermodynamically stable and their electronic and transport properties are strongly dependent on the core $[V(Bz)_2]_n$ nanowire. Interestingly, $[V(Bz)_2]_n$@SWBNNT and $[V(Bz)_2]_n$@DWBNNT are found to be robust quasi half metals.

2. Models and computational methods

SWBNNT (9, 9) are selected as prototype host single-walled nanotubes. For DWBNNT, inner (9, 9) and outer (14, 14) BNNTs are employed. The inner diameters of such SWBNNT and DWBNNT are large enough to accommodate $[V(Bz)_2]_n$. For computing electronic structures, the infinite $[V(Bz)_2]_n$@SWBNNT and $[V(Bz)_2]_n$@DWBNNT systems are modeled using the periodic condition in the axial direction. For computing transport properties, the two-probe devices are adopted. As a benchmark test, we have computed electronic and transport properties for pure SWBNNT, DWBNNT, and bare $[V(Bz)_2]_n$ systems.

For periodic systems, the supercell of $[V(Bz)_2]_n$@SWBNNT contains 144 atoms of BNNT and two units of $V(Bz)_2$ (i.e., $[V(Bz)_2]_2$) (Fig. 1), and that of $[V(Bz)_2]_n$@DWBNNT contains 224 atoms of outer BNNT layer, 144 atoms of inner BNNT layer, as well as two units of $V(Bz)_2$. This is because that the lattice parameter of the $[V(Bz)_2]_2$ (~9.69 Å) nearly matches the lattice parameter of the supercell of S(D)WBNNT (~9.84 Å). In addition, such a supercell containing two V atoms can be used to study magnetic coupling between V atoms. The nanocables are separated by 15 Å vacuum to neglect tube-tube interaction. All the periodic systems are fully optimized until the maximum absolute force is less than 0.02 eV/Å.

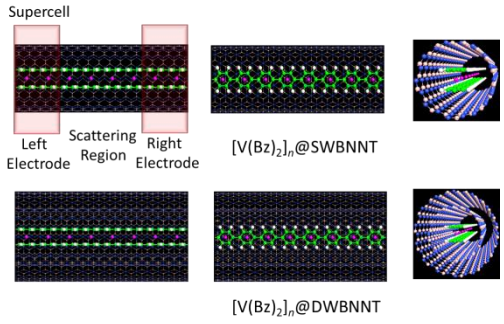

Fig. 1. Optimized structures of $[V(Bz)_2]_n$@SWBNNT and $[V(Bz)_2]_n$@DWBNNT. $[V(Bz)_2]_n$@SWBNNT also illustrates the two - probe devices for electron transport computation

For the two-probe devices, we take two optimized supercells as the central scatter region, i.e., $[V(Bz)_2]_4$@SWBNNT or $[V(Bz)_2]_4$@DWBNNT for the two-probe devices. The scatter region is long enough (>17 Å) to separate the left and right electrodes. To compute intrinsic transport properties of the nanocables, we select one supercell as each of the two opposing electrodes (Fig. 1). Transport current is computed by changing the applied bias in the step of 0.2 V in the range of -1.0~1.0 V.

All the computations for both infinitely long and two-probe systems are performed using combined density functional theory (DFT) and nonequilibrium Green's function (NEGF) methods, implemented in the software package Atomistix ToolKit (ATK) [34-37]. A generalized gradient approximation (GGA) within the Perdew-Burke-Ernzerhof (PBE) formalism is employed to describe the exchange correlations between electrons. Spin polarization of V atom is considered in all calculations. The on-site correlation effects among 3d electrons of V atom are accounted for by using the GGA + U scheme [37], where the parameter U is set to be 3.5 eV [38]. A double-ζ basis with polarization (DZP) is used for all atoms. A (1×1×100) *k*-point in string Brillouin zone (*x*, *y*, *z* directions, respectively) is adopted, and 150 Ry cutoff energy is applied to describe the periodic wave function.

3. Results and discussions

First, we show results of geometry, magnetism, and band structures of the infinitely long nanocables of $[V(Bz)_2]_4$@SWBNNT and $[V(Bz)_2]_4$@DWBNNT, followed by transport properties computed based on their two-probe devices. The results of pure SWBNNT, DWBNNT, and $[V(Bz)_2]_n$ are also given for comparison.

3.1. Stability and geometry

Fig. 1 shows optimized structures of $[V(Bz)_2]_4$@SWBNNT and $[V(Bz)_2]_4$@DWBNNT nanocables. Their computed total energies per supercell are listed in Table 1. The antiferromagnetic (AFM) state and the ferromagnetic (FM) state of the two V atoms are both considered. Notably, the two nanocables $[V(Bz)_2]_4$@SWBNNT and $[V(Bz)_2]_4$@DWBNNT favor the FM V-V coupling as reflected from the lower energy of the FM state compared to the AFM state. Hereafter, we mainly focus on the FM state of these nanocables and discuss associated electronic and transport properties.

Table 1. Calculation results for $[V(Bz)_2]_n$, $[V(Bz)_2]_n$@SWBNNT, and $[V(Bz)_2]_n$@SWBNNT[a]

Species	$E_{Tot,FM}$ /eV	$E_{Tot,AFM}$/eV	$\Delta E_{FM\text{-}AFM}$/eV	$\Delta E_{r,FM}$/eV	J/eV	$T_{c(N)}$/K	S/μ_B
$[V(Bz)_2]_n$	-7874.9980	-7874.8519	-0.146	-	0.146	566.3	2.6
$[V(Bz)_2]_n$@SWBNNT	-33195.3089	-33195.0121	-0.297	-0.615	0.297	1150.4	2.6
$[V(Bz)_2]_n$@SWBNNT	-72588.0222	-72587.7104	-0.312	-0.271	0.312	1208.5	2.6

[a] For per supercell, total energies in the FM or AFM state ($E_{Tot,FM}$, $E_{Tot,AFM}$), the energy difference between FM and AFM states ($\Delta E_{FM\text{-}AFM}$), the reaction energy in the FM state ($\Delta E_{r,FM}$), the exchange parameter (J), the Curie or Neél temperatures ($T_{C(N)}$), and the total magnetic moment (S).

Chemical stability for encapsulated $[V(Bz)_2]_n$ is evaluated by computing the reaction energy per supercell for the net reaction, NT+ $[V(Bz)_2]_2 \rightarrow [V(Bz)_2]_2$@NT - ΔE_r, where NT represents the nanotube in a supercell. Here, the computed reaction energies ΔE_r are -0.615 and -0.271 eV for $[V(Bz)_2]_4$@SWBNNT and $[V(Bz)_2]_4$@DWBNNT, respectively (Table 1). The negative values indicate exothermic reactions. Hence, incorporation of $[V(Bz)_2]_n$ into SWBNNT and DWBNNT is energetically favorable.

The optimized supercell length in the axial direction (L), the radii of the outer BNNT layer (R_{out}), the radii of the inner BNNT layer (R_{in}), the neighboring V-V distances ($r_{V\text{-}V}$), the Bz-V distances ($r_{Bz\text{-}V}$), the interlayer distances between the outer and inner BNNT layers ($r_{out\text{-}in}$), and the nearest Bz-BNNT distances ($r_{Bz\text{-}NT}$) for $[V(Bz)_2]_n$@SWBNNT and $[V(Bz)_2]_n$@DWBNNT are given in Table 2. Incorporation of the $[V(Bz)_2]_n$ into BNNT causes no changes in supercell length as reflected from the identical values of L compared to the bare BNNT. The outer radii R_{out} and the inner radii R_{in} of $[V(Bz)_2]_n$@SWBNNT and $[V(Bz)_2]_n$@DWBNNT are slightly expanded compared with pure SWBNNT and DWBNNT, respectively. The inner BNNT layer and the outer BNNT layer of both DWBNNT and $[V(Bz)_2]_n$@DWBNNT are separated by about a 3.58 Å interval, suggesting a Van der Waals interlayer interaction. The neighboring V-V separations in $[V(Bz)_2]_n$@SWBNNT and $[V(Bz)_2]_n$@DWBNNT are slightly elongated by 0.076 Å comparing with bare $[V(Bz)_2]_n$. The V-Bz distances in $[V(Bz)_2]_n$@SWBNNT and $[V(Bz)_2]_n$@DWBNNT are around 1.74 Å, a little longer than that for experimental observed dimer $V(Bz)_2$ (1.66 Å) [39]. The shortest distances between Bz and BNNT $r_{Bz\text{-}NT}$ are 4.742 - 4.746 Å.

Table 2. Calculation Geometries for Supercells of SWBNNT, DWBNNT, $[V(Bz)_2]_n$, $[V(Bz)_2]_n$@SWBNNT, and $[V(Bz)_2]_n$@SWBNNT[a]

Species	L/Å	R_{out}/Å	R_{in}/Å	$r_{V\text{-}V}$/Å	$r_{out\text{-}in}$/Å	$r_{Bz\text{-}V}$/Å	$r_{Bz\text{-}BNNT}$/Å
SWBNNT	9.844	-	12.923	-	-	-	-
DWBNNT	9.844	20.109	12.950	-	3.580	-	-
$[V(Bz)_2]_n$	9.693	-	-	4.846	-	1.749	-
$[V(Bz)_2]_n$@SWBNNT	9.844	-	12.965	4.922	-	1.749	4.742
$[V(Bz)_2]_n$@DWBNNT	9.844	20.124	12.972	4.922	3.576	1.741	4.746

[a] The optimized supercell length in the axial direction (L), the radii of the outer BNNT layer (R_{out}), the radii of the inner BNNT layer (R_{in}), the neighboring V-V distances ($r_{V\text{-}V}$), the Bz-V distances ($r_{Bz\text{-}V}$), the interlayer distances between the outer and inner BNNT layers ($r_{out\text{-}in}$), and the nearest Bz-BNNT distances ($r_{Bz\text{-}BNNT}$).

3.2. Band structures

Fig. 2 displays spin-polarized band structures and the average projected density of states (PDOS) of each element for pure $[V(Bz)_2]_n$, together with the corresponding Kohn-Sham orbitals at the Γ point near the Fermi level (E_f). In the spin-up state, the V 3d states open a band gap of about 1.87 eV, suggesting an insulation

character. Evidently, in the spin-down state, a band crosses the E_f, showing a metallic character. Therefore, the $[V(Bz)_2]_n$ nanowire exhibits a half-metallic property. This result is very similar to that of the vanadium-benzene multidecker nanowire $(VBz)_n$, which is identified to be a half metal by experimental observations [26] and theoretical investigations [27-29]. Such fascinating property of $[V(Bz)_2]_n$ provides another good candidate for exploring ingenious electronics devices.

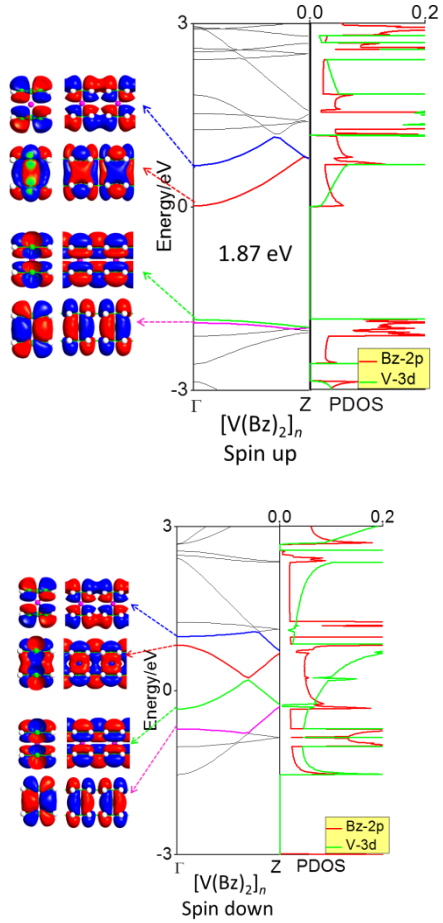

Fig. 2. Computed band structures and PDOS of $[V(Bz)_2]_n$ and the Kohn-Sham orbitals corresponding to the energy levels (highlighted in color lines) near E_f at the Γ point. The iso-surface value is 0.005 (e/Å^3)

In Fig. 3, computed band structures of pure SWBNNT and DWBNNT are plotted along with the associated Kohn-Sham orbitals near the E_f. For pure SWBNNT, as expected, the valence band is separated from the conduction band by a large band gap of 4.64 eV. By comparing Fig. 4 with Fig. 2, we find that the bands originated from the $[V(Bz)_2]_n$ are little affected even when inside the SWBNNT. In the spin-up state of $[V(Bz)_2]_n$@SWBNNT, the $[V(Bz)_2]_n$ bands are sandwiched between the valence band and conduction band of SWBNNT. As a result, the band gap of $[V(Bz)_2]_n$@SWBNNT (1.86 eV) is close to that of pure $[V(Bz)_2]_n$ (1.87 eV), much smaller than pure SWBNNT (4.64 eV). In the spin-down state, some $[V(Bz)_2]_n$ bands fall in the band gap region of SWBNNT and one crosses the E_f, very similar to the case of pure $[V(Bz)_2]_n$. As such, the $[V(Bz)_2]_n$ core can offer a metal-like transport path. In fact, the PDOS in Fig. 4 also demonstrates the band structure of $[V(Bz)_2]_n$@SWBNNT. The SWBNNT retains the insulating property in $[V(Bz)_2]_n$@SWBNNT as the SWBNNT PDOS are far away from the E_f. Corresponding PDOS peaks stemming from $[V(Bz)_2]_n$ appear near the E_f associated with the band positions in both spin-up and spin-down states. Therefore, $[V(Bz)_2]_n$@SWBNNT can be rendered half-metallic character arising from the core $[V(Bz)_2]_n$.

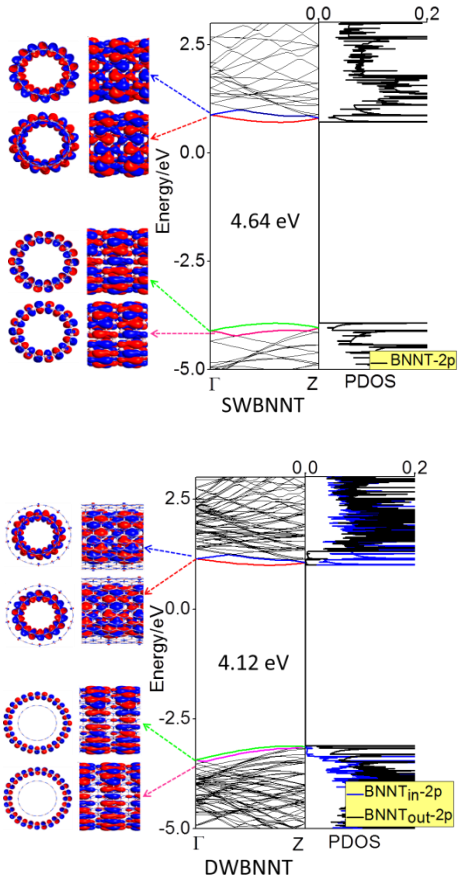

Fig. 3. Computed band structures and PDOS of SWBNNT and DWBNNT and the Kohn-Sham orbitals corresponding to the energy levels (highlighted in color lines) near E_f at the Γ point. The iso - surface value is 0.005 (e/Å^3)

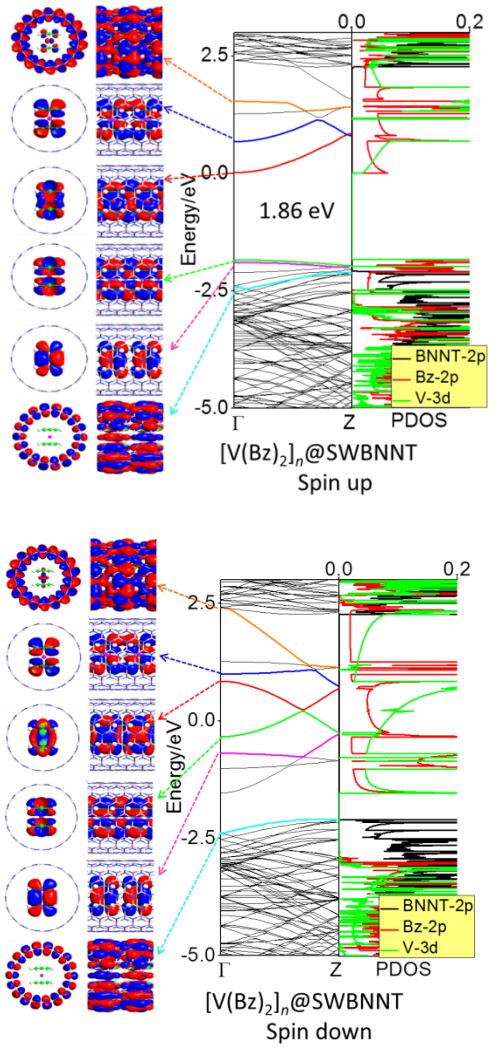

Fig. 4. Computed band structures and PDOS of $[V(Bz)_2]_n$@SWBNNT and the Kohn-Sham orbitals corresponding to the energy levels (highlighted in color lines) near E_f at the Γ point. The iso - surface value is 0.005 (e/Å^3)

As to pure DWBNNT (Fig. 5), the valence band originates from the outer layer, while the conduction band comes from the inner layer, and hence, electron transport in DWBNNT mainly undertakes an indirect mechanism through electron hopping form outer layer to inner layer. When $[V(Bz)_2]_n$ is encapsulated into DWBNNT, a similar case to $[V(Bz)_2]_n$@SWBNNT is found for $[V(Bz)_2]_n$@DWBNNT. That is, the spin-up state shows an insulator character while the spin-down state shows a metallic character. $[V(Bz)_2]_n$@SWBNNT and $[V(Bz)_2]_n$@DWBNNT span a same band gap (1.86 eV) in their spin-up state even though DWBNNT has a smaller band gap (4.12 eV) than SWBNNT (4.64 eV).

Overall, both $[V(Bz)_2]_n$@SWBNNT and $[V(Bz)_2]_n$@DWBNNT inherit the intriguing half-metallic property of $[V(Bz)_2]_n$ and the BN sheath provides mechanical and electric isolation to the core $[V(Bz)_2]_n$.

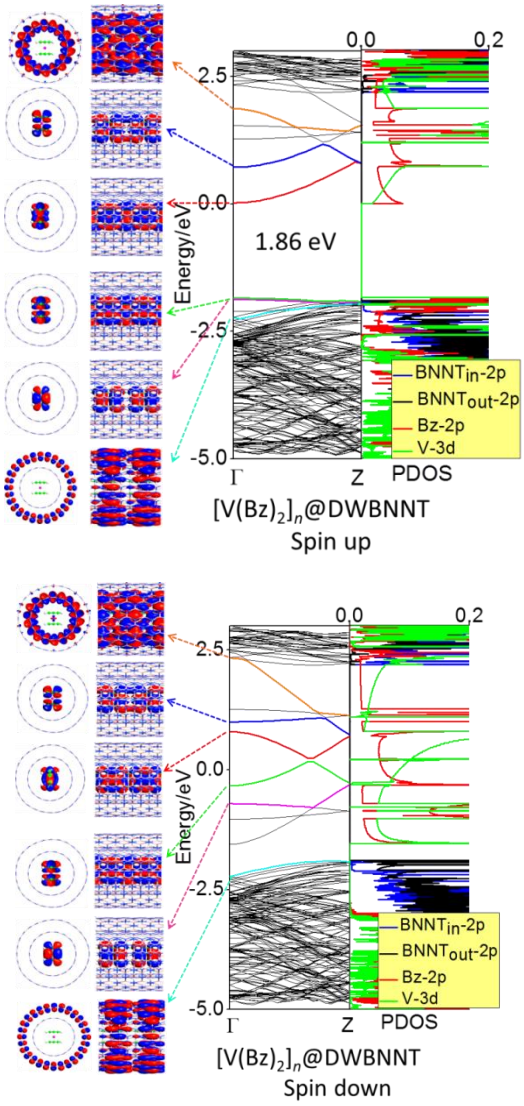

Fig. 5. Computed band structures and PDOS of $[V(Bz)_2]_n$@DWBNNT and the Kohn-Sham orbitals corresponding to the energy levels (highlighted in color lines) near E_f at the Γ point. The iso - surface value is 0.005 (e/Å^3)

3.3. Magnetic properties

As shown in Table 1, $[V(Bz)_2]_n$@SWBNNT and $[V(Bz)_2]_n$@DWBNNT nanocables all favor the FM ground state and have same magnetic moments *S* for each supercell (2.6 μ_B), equal to the pure $[V(Bz)_2]_n$. This value is larger than the mutidecker sandwich-like $[V(Bz)]_n$ nanowire (*S*=2.0) [29]. The magnetic behavior of $[V(Bz)_2]_n$@SWBNNT and $[V(Bz)_2]_n$@DWBNNT nanocables is also reflected by uneven PDOS distribution in the spin-up and spin-down states as shown in Fig. 4 and

5. The spin polarization is mainly due to the V atoms. The exchange parameter J, which can be estimated by the energy difference between AFM and FM configurations, is about 0.297 and 0.312 eV per supercell (containing two V atoms) for $[V(Bz)_2]_n$@SWBNNT and $[V(Bz)_2]_n$@DWBNNT, respectively (Table 1). We also estimate the Curie or Neél temperatures, $T_{C(N)}$, of the nanocables using the formula $3/2k_BT_{C(N)} = J/2$. The estimated $T_{C(N)}$ for $[V(Bz)_2]_n$@SWBNNT and $[V(Bz)_2]_n$@DWBNNT amounts up to over 1000 K (Table 1), much higher than that of bare $[V(Bz)_2]_n$ (566 K), suggesting that the FM state of the two nanocables can be rather stable even at elevated temperatures. Therefore, $[V(Bz)_2]_n$@SWBNNT and $[V(Bz)_2]_n$@DWBNNT are potential candidates as magnetic nanopart.

3.4. Transport properties

To analyze the effect of core $[V(Bz)_2]_n$ on the transport properties of the two nanocables, we construct a model system such that two unit cells, i.e., $[V(Bz)_2]_4$@SWBNNT or $[V(Bz)_2]_4$@DWBNNT, are sandwiched between two electrodes, forming two-probe device as described in Section 2 (Fig. 1). Computation results suggest that electric conductivities of the two-probe devices are consistent with the electronic structures of the corresponding infinitely long systems.

The computed *I-V* curves based on the two-probe devices are shown in Fig. 6(a). SWBNNT and DWBNNT have nearly zero current supporting their insulating character. Notably, the nanocables $[V(Bz)_2]_n$@SWBNNT and $[V(Bz)_2]_n$@DWBNNT display almost the same conductivity as pure $[V(Bz)_2]_n$, indicating that the core $[V(Bz)_2]_n$ plays the major role in electron transport after enclosed in SWBNNT or DWBNNT, consistent with computed electronic structures. Fig. 7 gives the transmission spectra (TS) of SWBNNT, DWBNNT, $[V(Bz)_2]_n$, $[V(Bz)_2]_n$@SWBNNT, and $[V(Bz)_2]_n$@DWBNNT. For SWBNNT and DWBNNT, no TS peak appears at E_f at 0.0 V bias voltage (Fig. 7(a)) or within the bias window at 1.0 V bias voltage (Fig. 7(b)), while $[V(Bz)_2]_n$, $[V(Bz)_2]_n$@SWBNNT, and $[V(Bz)_2]_n$@DWBNNT have the same magnitude of TS peak at E_f at 0.0 V bias voltage (Fig. 7(a)) or within the bias window at 1.0 V bias voltage (Fig. 7(b)). Here, the bias window refers to [-V/2, V/2] (indicated by wine lines in Fig. 7). Generally, only states within the bias window contribute to the current. This result again manifests the dominate role of core $[V(Bz)_2]_n$ in electron transporting. Furthermore, the voltage potentials are also shown in Fig. 8. Clearly, for $[V(Bz)_2]_n$@SWBNNT and $[V(Bz)_2]_n$@DWBNNT, the voltage potential drop takes place mainly upon core $[V(Bz)_2]_n$.

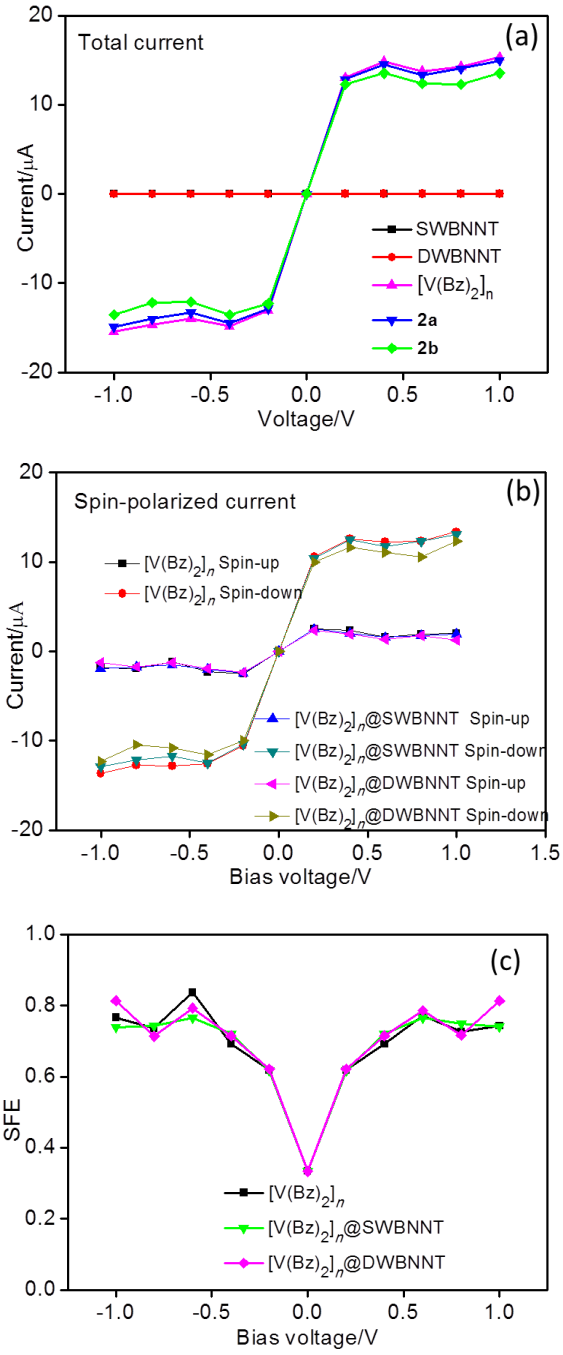

Fig. 6. (a) Total currents of SWBNNT, DWBNNT, $[V(Bz)_2]_n$, $[V(Bz)_2]_n$@SWBNNT, and $[V(Bz)_2]_n$@DWBNNT; (b) Spin-polarized currents of $[V(Bz)_2]_n$, $[V(Bz)_2]_n$@SWBNNT, and $[V(Bz)_2]_n$@DWBNNT; and (e) SFE curves of $[V(Bz)_2]_n$, $[V(Bz)_2]_n$@SWBNNT, and $[V(Bz)_2]_n$@DWBNNT

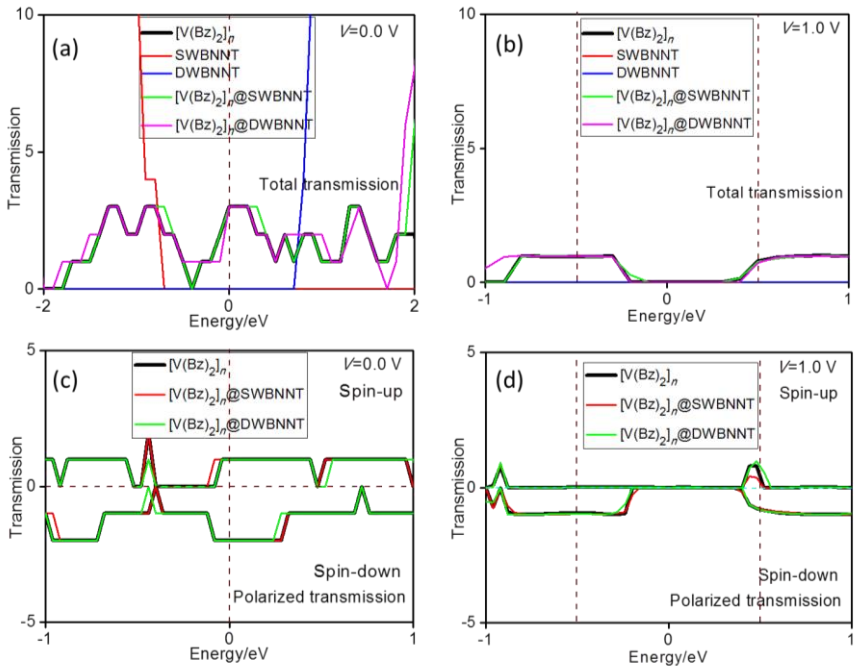

Fig. 7. (a) and (b) Total transmission spectra of $[V(Bz)_2]_n$, SWBNNT, DWBNNT, $[V(Bz)_2]_n$@SWBNNT, and $[V(Bz)_2]_n$@DWBNNT two-probe devices at bias voltage of 0.0 and 1.0 V, respectively; (c) and (d) Polarized transmission spectra of $[V(Bz)_2]_n$, $[V(Bz)_2]_n$@SWBNNT, and $[V(Bz)_2]_n$@DWBNNT two - probe devices at bias voltage of 0.0 and 1.0 V, respectively; The vertical wine lines in (a) and (c) refer to the E_f, and in (b) and (d) refer to the bias window

For FM $[V(Bz)_2]_n$, $[V(Bz)_2]_n$@SWBNNT, and $[V(Bz)_2]_n$@DWBNNT systems the spin-up current ($I_\uparrow$) and spin-down current ($I_\downarrow$) are computed. The conductivities are spin-state dependent within the bias range of -1.0~1.0 V. The spin-down state gives a higher conductivity than the spin-up state (Fig. 6(b)), consistent with electronic structures of their infinitely long systems.

The spin filter efficiency (SFE) at zero bias voltage can be evaluated from the transmission by using the formula

$$\mathrm{SFE} = \frac{T_\downarrow(E_\mathrm{f}) - T_\uparrow(E_\mathrm{f})}{T_\uparrow(E_\mathrm{f}) + T_\downarrow(E_\mathrm{f})} \quad (1)$$

where $T_\downarrow(E_\mathrm{f})$ and $T_\uparrow(E_\mathrm{f})$ are the transmission coefficient of spin-down and spin-up channel at E_f under zero bias voltage. At a bias voltage, the SFE is defined as

$$\mathrm{SFE} = \frac{I_\downarrow - I_\uparrow}{I_\uparrow + I_\downarrow} \quad (2)$$

where $I_\downarrow$ and $I_\uparrow$ represent spin-down and spin-up current, respectively.

The SFE curves under different bias for $[V(Bz)_2]_n$, $[V(Bz)_2]_n$@SWBNNT, and $[V(Bz)_2]_n$@DWBNNT systems are shown in Fig. 6(c). $[V(Bz)_2]_n$@SWBNNT and $[V(Bz)_2]_n$@DWBNNT have comparable SFE values as pure $[V(Bz)_2]_n$, which are higher than 60%. Therefore, these two nanocables exhibit spin-polarized transport properties, which may be exploited as a new kind of spin filter.

The spin-polarized transport phenomenon of $[V(Bz)_2]_n$, $[V(Bz)_2]_n$@SWBNNT, and $[V(Bz)_2]_n$@DWBNNT can be further confirmed by the TS distribution in Fig. 7(c,d). At 0.0 V bias voltage, the spin-down state of $[V(Bz)_2]_n$, $[V(Bz)_2]_n$@SWBNNT, $[V(Bz)_2]_n$@DWBNNT shows a larger TS magnitude than the spin-up state at the E_f (Fig. 7(c)). Similarly, under 1.0 V bias voltage, the spin-down state presents a larger TS contribution than the spin-up state within the bias window (Fig. 7(d)). Therefore, $[V(Bz)_2]_n$, $[V(Bz)_2]_n$@SWBNNT, and $[V(Bz)_2]_n$@DWBNNT should have a high value of >60% of SFE.

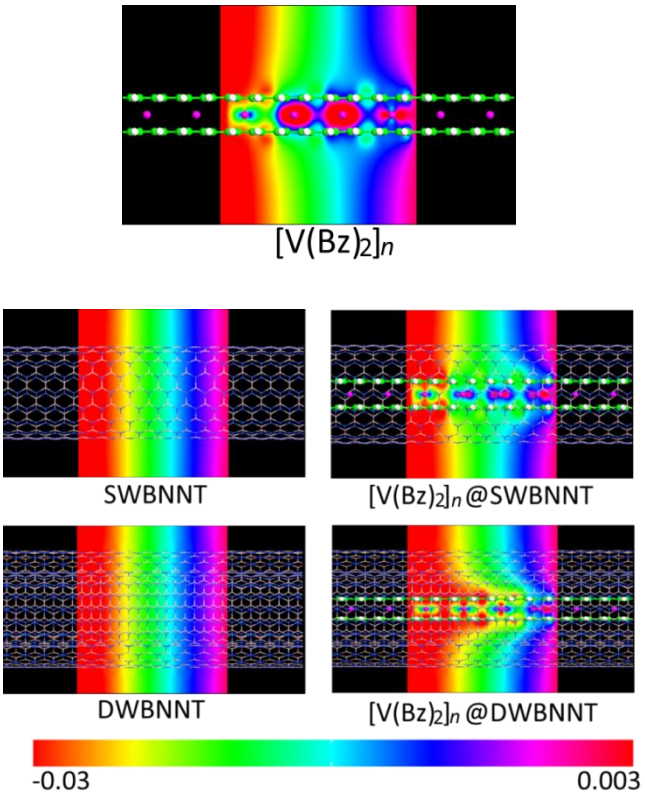

Fig. 8. Voltage potential at 1.0 V for two-probe devices of $[V(Bz)_2]_n$, SWBNNT, DWBNNT, $[V(Bz)_2]_n$@SWBNNT, and $[V(Bz)_2]_n$@DWBNNT

4. Conclusions

We have investigated electronic and transport properties of a novel form of $[V(Bz)_2]_n$@SWBNNT and $[V(Bz)_2]_n$@DWBNNT nanocables by means of DFT and NEGF methods. We find that endohedral encapsulation of $[V(Bz)_2]_n$ into SWBNNT or DWBNNT is energetically favorable. Both $[V(Bz)_2]_n$@SWBNNT and $[V(Bz)_2]_n$@DWBNNT exhibit magnetism. More importantly, the ferromagnetic state of the two nanocables is predicted to have a very high Curie or Neél temperature of over 1000 K, suggesting a potential candidate as magnetic nanopart. Transport properties of $[V(Bz)_2]_n$@SWBNNT and $[V(Bz)_2]_n$@DWBNNT are mainly controlled by the core $[V(Bz)_2]_n$ nanowire. Their conductivities are dependent on the spin state: spin-down state gives a higher conductivity than the spin-up state, rendering them a half-metallic character. Values of the spin-filter efficiency of $[V(Bz)_2]_n$@SWBNNT and $[V(Bz)_2]_n$@DWBNNT amount to more than 60%, which may be viewed as a new kind of spin filter. Encapsulating $[V(Bz)_2]_n$ into either SWBNNT or DWBNNT can effectively tune electronic and transport properties and these nanocables can be potentially used as functional nanodevices.

Acknowledgments

GLZ is supported by the NSFC (grant No. 51473042). SY is supported by the SF for youth reserve talent of Harbin of China (grant No. 2014RFQXJ075), the NSF of Heilongjiang Province of China (grant No. E201236), and the foundation for the department of education of Heilongjiang Province of China (grant No. 12521074).

References

[1] K. H. He, G. Zheng, G. Chen, M. Wan, G. F. Ji, Physica B **403**(23-24), 4213 (2008).
[2] C. K. Yang, J. Zhao, J. P. Lu, Phys. Rev. B **74**(23), 235445 (2006).
[3] K. B. Shelimov, M. Moskovits, Chem. Mater. **12**(1), 250 (2000).
[4] C. Tang, Y. Bando, D. Golberg, X. Ding, S. Qi, J. Phys. Chem. B **107**(27), 6539 (2003).
[5] D. Golberg, F. F. Xu, Y. Bando, Appl. Phys. A **76**(4), 479 (2003).
[6] R. Ma, Y. Bando, T. Sato, Chem. Phys. Lett. **350**(1-2), 1 (2001).
[7] N. Koi, T. Oku, M. Nishijima, Solid State Commun. **136**(6), 342 (2005).
[8] T. Oku, N. Koi, I. Narita, K. Suganuma, M. Nishijima, Mater. Trans. **48**(4), 722 (2007).
[9] G. Dmitri, B. Yoshio, K. Keiji, S. Tadao, J. Nanosci. Nanotechnol. **1**, 49 (2001).
[10] W. Q. Han, C. W. Chang, A. Zettl, Nano Lett. **4**(7), 1355 (2004).
[11] C. Tang, Y. Bando, T. Sato, K. Kurashima, J. Mater. Chem. **12**(6), 1910 (2002).
[12] Y. C. Zhu, Y. Bando, D. F. Xue, F. F. Xu, D. Golberg, J. Am. Chem. Soc. **125**(47), 14226 (2003).
[13] Y. Li, P. S. Dorozhkin, Y. Bando, D. Golberg, Adv. Mater. **17**(5), 545 (2005).
[14] T. Sugino, S. Kawasaki, K. Tanioka, J. Shirafuji, Appl. Phys. Lett. **71**(18), 2704 (1997).
[15] C. Tang, Y. Bando, Appl. Phys. Lett. **83**(4), 659 (2003).
[16] W. Q. Han, A. Zettla, Appl. Phys. Lett. **81**(26), 5051 (2002).
[17] C. Kimura, T. Yamamoto, T. Suginoa, J. Vac. Sci. Technol. B **21**(1), 544 (2003).
[18] E. W. S. Caetano, V. N. Freire, G. A. Farias, E. F. da Silva Jr, Appl. Surf. Sci. **234**(1-4), 50 (2004).
[19] W. S. Jang, S. Y. Kim, J. Lee, J. Park, C. J. Park, C. J. Lee, Chem. Phys. Lett. **422**(1-3), 41 (2006).
[20] D. Golberg, Y. Bando, A. Prokofiev, J. Q. Hu, L. W. Yin, J. H. Zhan, Appl. Phys. A **85**(3), 265 (2006).
[21] H. S. Song, J. Zhang, J. Lin, S. J. Liu, J. J. Luo, Y. Huang, E. M. Elssfah, A. Elsanousi, X. X. Ding, J. M. Gao, C. Tang, J. Phys. Chem. C **111**(3), 1136 (2007).
[22] S. Okada, S. Saito, A. Oshiyama, Phys. Rev. B

65(16), 165410 (2002).
[23] G. G. Fuentes, E. Borowiak-Palen, T. Pichler, X. Liu, A. Graff, G. Behr, R. J. Kalenczuk, M. Knupfer, J. Fink, Phys. Rev. B **67**(3), 035429 (2003).
[24] D. Golberg, Y. Bando, C. Tang, C. Zhi, Adv. Mater. **19**(18), 2413 (2007).
[25] D. Golberg, M. Mitome, Y. Bando, C. Tang, C. Zhi, Appl. Phys. A **88**(2), 347 (2007).
[26] K. Miyajima, A. Nakajima, S. Yabushita, M. B. Knickelbein, K. Kaya, J. Am. Chem. Soc. **126**(41), 13202 (2004).
[27] H. Xiang, J. Yang, J. G. Hou, Q. Zhu, J. Am. Chem. Soc. **128**(7), 2310 (2006).
[28] J. Wang, P. H. Acioli, J. Jellinek, J. Am. Chem. Soc. **127**(9), 2812 (2005).
[29] V. V. Maslyuk, A. Bagrets, V. Meded, A. Arnold, F. Evers, M. Brandbyge, T. Bredow, I. Mertig, Phys. Rev. Lett. **97**(9), 097201 (2006).
[30] T. Kurikawa, H. Takeda, M. Hirano, K. Judai, T. Arita, S. Nagao, A. Nakajima, K. Kaya, Organometallics **18**(8), 1430 (1999).
[31] T. J. Katz, N. Acton, J. Am. Chem. Soc. **94**, 3281 (1972).
[32] X. Wu, X. C. Zeng, J. Am. Chem. Soc. **131**(40), 14246 (2009).
[33] X. Wang, X. Zheng, Z. Zeng, Appl. Phys. Lett. **103**(3), 032404 (2013).
[34] J. Taylor, H. Guo, J. Wang, Phys. Rev. B **63**(24), 245407 (2001).
[35] M. Brandbyge, J. L. Mozos, P. Ordejón, J. Taylor, K. Stokbro, Phys. Rev. B **65**(16), 165401 (2002).
[36] J. M. Soler, E. Artacho, J. D. Gale, A. García, J. Junquera, P. Ordejón, D. Sánchez-Portal, J. Phys. Condens. Matter. **14**, 2745 (2002).
[37] ATK, Version 13.8, atomistix a/s (2013) www.quantumwise.com.
[38] J. K. Heather, C. Matteo, A. S. Damian, M. Nicola, Phys. Rev. Lett. **97,** 103001 (2006).
[39] E. L. Muetterties, J. R. Bleeke, E. J. Wucherer, T. A. Albright, Chem. Rev. **82**, 499 (1982).

*Corresponding author: guiling-002@163.com